Beamforming with metagratings at microwave frequencies : design procedure and experimental demonstration

Vladislav Popov, Fabrice Boust, Shah Nawaz Burokur

Beamforming with metagratings at microwave frequencies: design procedure and experimental demonstration

Vladislav Popov, Fabrice Boust, *Member, IEEE,* and Shah Nawaz Burokur, *Member, IEEE*

***Abstract*—As opposed to metasurfaces, metagratings represent themselves sparse arrangements of scatterers. Established rigorous analytical models allow metagratings to overcome performance of metasurfaces in beam steering applications while handling less degrees of freedom. In this work we deal with reflective metagratings that have only as few as one degree of freedom (represented by a reactively loaded thin wire) per each propagating diffraction order. We present a detailed design procedure and fabrication of three experimental samples capable of establishing prescribed diffraction patterns. The samples are experimentally studied in an anechoic chamber dedicated to radar-cross-section bistatic measurements and results are compared with three-dimension full wave numerical simulations. We identify and analyze factors affecting operating frequency range of metagratings, suggest a strategy to increase the bandwidth.**

***Index Terms*—Electromagnetic metasurfaces, diffraction, metagratings, beam steering, reflector antennas.**

I. Introduction

A diffraction grating, defined as a periodic optical structure with infinite extent in one direction diffracts waves incident on its surface [1]. Being imposed by the periodicity of a grating, which can be of the order of a free-space wavelength or greater, an incident wave is scattered as propagating diffraction orders only in certain directions. Concerning their applications, diffraction gratings have been widely used in laser resonators to tune and narrow lasing bandwidth [2], [3]. Blazed or echelette gratings [4], [5], [6] capable of scattering an incident wave into a specific diffraction order have been applied in frequency-scanning reflector antennas [7], [8], [9], [10] and for radar cross section (RCS) reduction [11], [12] at microwave frequencies and in Littrow mount external cavity lasers in optics [13]. Classical blazed gratings are three-dimensional (3D) structures that generally take the form of right-angle sawtooths [14] and rectangular grooves [5].

In the last few years, 2D metamaterials, also known as metasurfaces [15], have been applied to mimic blazed gratings functionality [16]. Metasurfaces representing themselves as very thin structures have been proposed as planar alternatives to metamaterials to exhibit light manipulation possibilities in various frequency domains, extending from microwave to visible frequencies. Local magnitude and phase of reflection and/or transmission coefficients of a metasurface can be controlled, and can thus be used to manipulate scattered wavefront of an incident beam. As such, metasurfaces have been used to perform functions including anomalous reflection and refraction [17], [18], [19], [20], [21], [22], deflection [23], [24], [25], [26], lensing [23], [24], [27], [28], [29], [30], thin-film cloaking [31], [32], [33], coupling of propagating waves to surface waves [34], [35], optical vortex beams generation [36], [37], [38], [39], and holographic imaging [40], [41], [42], [43], [44], [45], to name a few.

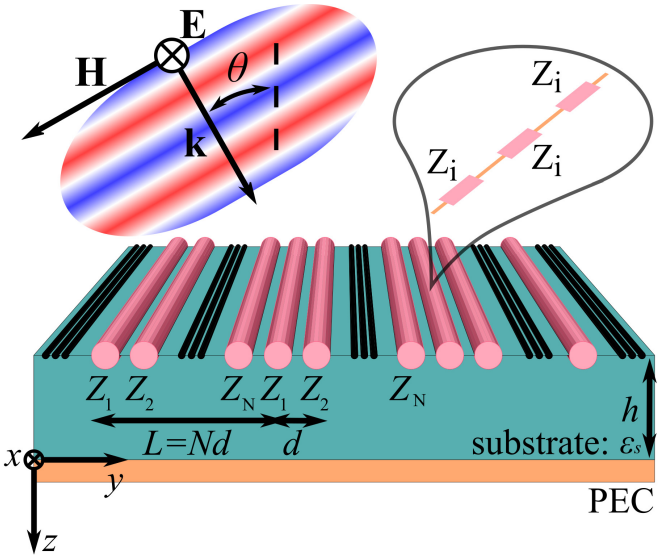

Fig. 1. Schematic diagram of the system under consideration: a periodic array of loaded thin wires (pink cylindrical lines) placed on PEC-backed dielectric substrate having permittivity ε_s and thickness h. The array is excited by a TE-polarized plane wave incident at angle θ.

Most of the metasurface-based wavefront manipulation geometries rely on the generalized laws of reflection and refraction presented in Ref. [17]. However several studies have shown that this approach suffer from low efficiency, particularly in configurations where extreme wave manipulation is considered (see, e.g., Refs. [46], [47], [48]). Moreover, implementation of field transformations into physical metasurface structures can reveal to be highly challenging and drawbacks concerning optimization time, design complexity of subwavelength periodically arranged resonant meta-atoms and material losses still exist.

Very recently, the concept of metagratings evolved from

V. Popov is with SONDRA, CentraleSupélec, Université Paris-Saclay, F-91190, Gif-sur-Yvette, France (e-mail: uladzislau.papou@centralesupelec.fr).

F. Boust is with SONDRA, CentraleSupélec, Université Paris-Saclay, F-91190, Gif-sur-Yvette, France and DEMR, ONERA, Université Paris-Saclay, F-91123, Palaiseau, France (e-mail: fabrice.boust@onera.fr).

S. N. Burokur is with LEME, UPL, Univ Paris Nanterre, F92410, Ville d'Avray, France (e-mail: sburokur@parisnanterre.fr).

classical diffraction gratings has been proposed as an interesting alternative to metasurfaces for boosting wavefront manipulation efficiency [49]. They are designed for diffraction engineering by cancelling a finite number of undesired propagating diffraction orders and allowing desired ones to radiate. In general, a metagrating is an array of scatterers (polarizable particles) separated by a distance of the order of the operating wavelength λ. The sparse arrangement of scatterers does not allow one describing metagratings in terms of local reflection and transmission coefficients (or surface impedances) as metasurfaces. In terms of meta-atoms, a metagrating consists of a limited number of meta-atoms in a supercell (period) compared to a metasurface which is composed of supercells incorporating numerous meta-atoms with subwavelength periodicity. Although metagratings can be considered as relatively simple systems in comparison to metasurfaces, functionalities such as perfect anomalous reflection and perfect beam splitting have been demonstrated in Refs. [49], [50], [51], [52], where three propagating diffraction orders were considered at most and were handled by only two degrees of freedom. In Refs. [53], [54], the concept was generalized and the possibility to fully control an arbitrary number of propagating diffraction orders by means of a specific number of degrees of freedom was demonstrated.

Essentially metagratings can be understood by considering an example of 1D metagratings represented by a periodic array of supercells composed of N thin wires each. An incident wave excites polarization line currents in the wires resulting in the scattered field represented by Floquet-Bloch modes which are defined by the period L of the array (i.e., the length of the supercell). In particular, the diffraction angles of the propagating diffraction orders can be found via the grating formula: $L(\sin[\theta_m] - \sin[\theta_i]) = m\lambda$, where m represents the number of an order and θ_i is the incidence angle of an impinging plane wave. Furthermore, a line current is mathematically represented by the 2D Dirac delta function $\delta(y, z)$ that allows one to find the scattered field analytically, i.e., to know the complex amplitudes of all diffraction orders (propagating and nonpropagating).

In what follows, we deal with a particular configuration of 1D metagratings when thin wires are placed on the top of a metal-backed dielectric substrate as illustrated in Fig. 1. A plane-wave illumination is assumed and the wires interact only with the TE-polarized field. As it was shown in the theoretical study [53], the complex amplitudes A_m^{TE} of the electric field of the reflected plane waves are given by the following expression:

$$A_m^{\mathrm{TE}} = -\frac{k\eta}{2L}\frac{(1+R_m^{\mathrm{TE}})e^{j\beta_m h}}{\beta_m}\sum_{q=1}^{N} I_q e^{j\xi_m(q-1)d} + \delta_{m0}R_0^{\mathrm{TE}}e^{2j\beta_0 h} \quad (1)$$

where k and η are respectively, the wavenumber and the characteristic impedance outside the substrate, $\xi_m = k\sin[\theta_i] + 2\pi m/L$ and $\beta_m = \sqrt{k^2 - \xi_m^2}$ represent respectively, the tangential and normal components of wavevector of the plane waves, and R_m^{TE} is the corresponding Fresnel's reflection coefficient. Equation (1) suggests that complex amplitudes of all M propagating diffraction orders can be set arbitrarily if there are at least $N = M$ line currents I_q in a supercell. Other parameters of the system, such as the parameters of the substrate and the distances between the line currents are assumed being fixed conversely to previously mentioned studies in Refs. [49], [50], [51], [52].

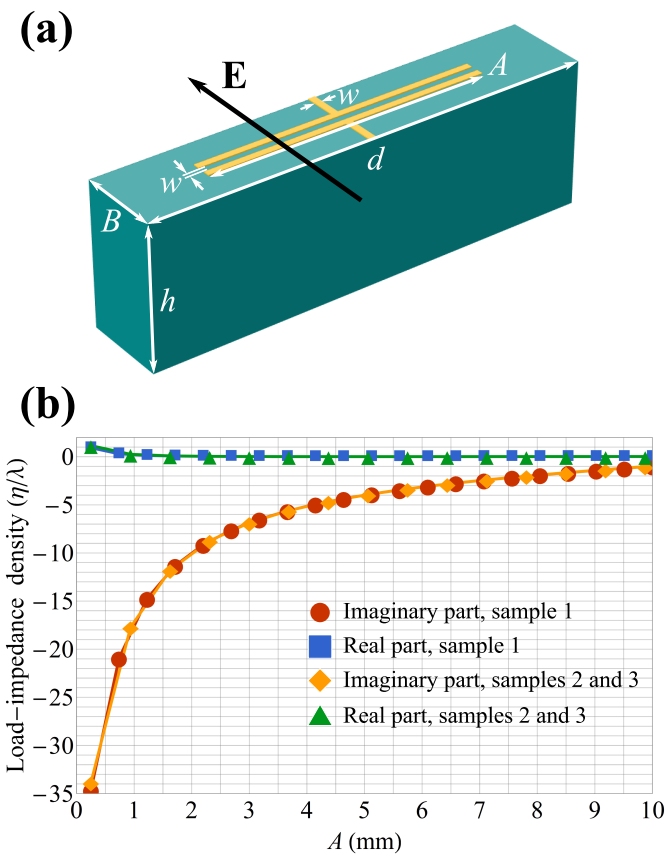

Fig. 2. (a) Schematic illustration of a capacitive unit cell: printed capacitance on top of a grounded dielectric substrate. (b) Load-impedance density of the printed capacitance extracted from specular reflection. $d \approx 11.6$ mm for the first sample and $d \approx 15.7$ mm in case of the second and third samples. Geometrical parameters are: $w = 0.25$ mm, $B = 3$ mm and $h = 5$ mm and operating frequency is set to 10 GHz.

Although here we focus on the TE polarization and reflective configuration of metagratings, the case of TM polarization can be studied similarly by means of duality relations (see, e.g., Refs. [55], [56]). The mathematical approach used in [53] to derive Eq. (1) can be straightforwardly generalized on transmissive-type metagratings, as the particular configuration studied in [57].

In this work, based on the theoretical study of Ref. [53], the design of simplified metagratings composed of the number of loaded wire as the considered number of propagating diffraction orders, is presented. The load-impedance densities of the wires are calculated and engineered from subwavelength wire elements. Measurements are performed on fabricated samples to experimentally validate the theoretical results . The rest of the paper is organized as follows. In Section II we provide the design methodology of the reflective-type metagratings. Section III is devoted to the discussion of the experimental results and their comparison to simulation results. In the

same Section we discuss the mechanism behind the observed wide-band response of the proposed metagratings (see also Refs. [51], [53]). Section IV concludes the paper.

II. DESIGN PROCEDURE

In order to be able to control the diffraction pattern with a metagrating one has to carefully engineer it. An appropriate dielectric substrate for a given frequency range is required. Its thickness h and relative permittivity ε_s should be carefully chosen in order to avoid excitation of waveguide modes [53]. These waveguide modes are analog of surface plasmon polaritons responsible for well-known grating anomalies (or Wood's anomalies). On the other hand, the presence of waveguide modes leads to divergence of certain Fresnel's reflection coefficients R_m^{TE} in Eq. (1), manifesting themselves in significant numerical errors. Thus, in order to select a good substrate for a given metagrating's period L, one can plot the absolute value of the first few Fresnel's reflection coefficients corresponding to nonpropogating diffraction orders as a function of the substrate's parameters (thickness and permittivity) and avoid poles. As a rule of thumb, a substrate with low permittivity and thickness of the order of $\lambda/(4\sqrt{\varepsilon_s})$ is a good candidate for the design of metagratings.

After selecting the correct substrate, the calculation of the characteristics of scatterers composing the metagrating has to be performed. Incident plane wave excites polarization line currents I_q in loaded thin wires that can be characterized by load-impedance Z_q and input-impedance Z_{in} densities. Each configuration of the diffraction pattern requires different set of load-impedance densities found from the Ohm's law:

$$Z_q I_q = E_q - Z_{in} I_q - \sum_{p=1}^{N} Z_{qp}^{(m)} I_p. \tag{2}$$

The right-hand side of Eq. (2) represents the total electric field at the location of the q^{th} wire (including the self-action $Z_{in}I_q$). Thus, $E_q = (1 + R_0^{\mathrm{TE}}) \exp[j\beta_0 h - j\xi_0(q-1)d]$ is the external electric field created by the incident wave $e^{-jk\sin\theta y - jk\cos\theta z + j\omega t}$ reflected from the substrate and the sum $\sum_{p=1}^{N} Z_{qp}^{(m)} I_p$ takes into consideration the mutual interactions of the q^{th} wire with the rest of the wires (infinite number) and the grounded substrate. The quantities $Z_{qp}^{(m)}$ are called as mutual-impedance densities. Generally, load-impedance densities calculated from Eq. (2) require engineering active and/or lossy response, i.e. $\Re[Z_q] \neq 0$. For instance, in order to perform a large angle nonspecular reflection by means of a $N = M$ metagrating, one has to cancel two propagating diffraction orders out of $M = 3$ available (as in the case of normal incidence). Then, the conditions $A_{-1}^{\mathrm{TE}} = 0$ and $A_0^{\mathrm{TE}} = 0$ leave one with only a single variable (being the phase of A_1^{TE}) that cannot be used to satisfy three different equations

$$\Re\left[\left(E_q - \sum_{p=1}^{N} Z_{qp}^{(m)} I_p\right) I_q^*\right] - \Re[Z_{in}]|I_q|^2 = 0 \tag{3}$$

providing reactive load-impedance densities (the asterisk stands for the complex conjugate). Equation (1) relates the complex amplitudes and currents, i.e. Eq. (3) can be rewritten in terms of A_m, with m numbering propagating diffraction orders.

TABLE I
PARAMETERS OF THE FABRICATED METAGRATINGS. THE INDEXES CORRESPOND TO THE NUMBERED UNIT CELLS IN FIGS. 3 (A)–(C).

Loads (η/λ)	Z_1	Z_2	Z_3	Z_4	Z_5
Sample 1	$-j30.3$	$-j6.35$	$-j1.57$	-	-
Sample 2	$-j3.77$	$-j0.43$	$-j31.2$	$-j7.06$	$-j5.27$
Sample 3	$-j3.75$	$-j4.84$	$j0.05$	$-j2.94$	$-j8.86$
Arm's length (mm)	A_1	A_2	A_3	A_4	A_5
Sample 1	0.37	3.25	8.70	-	-
Sample 2	5.23	11.2	0.33	2.91	3.90
Sample 3	5.25	4.22	12.3	6.28	2.27

In order to deal with $N = M$ passive and lossless metagratings, equation (3) has to be satisfied. To that end, spurious scattering in undesired propagating diffraction orders has to be permitted. By introducing scattering losses, we sacrifice the efficiency for sake of design that would require only reactive elements. An optimal configuration is achieved by numerically maximizing the power scattered in desired propagating diffraction orders while minimizing the left-hand-side of Eq. (3). It is worth to note that reflecting metasurfaces face the same difficulty (see for e.g., Refs. [46], [47]) with notable exception of Refs. [58], [59], which are rather special cases. Generally, the efficiency of nonspecular reflection is used to evaluate the performance of conventional reflectarrays, i.e., efficiency decreases when the angle of nonspecular reflection increases. However, highly efficient multichannel reflection can still be achieved as we demonstrate further.

Once Eq. (3) is satisfied and corresponding complex amplitudes are found, load-impedance densities are calculated from Eq. (2) and implemented by wire elements engineered at subwavelength scale. Although in a general case both capacitive and inductive loads might be required [54], only capacitive elements are necessary in the examples considered further for an operating frequency set to 10 GHz. It is assumed that the samples would be fabricated by means of the conventional printed-circuit-board (PCB) technology. Thus, thin wires are represented by metallic strips of width $w \ll \lambda$, thickness of $t_m = 35$ μm, and input-impedance density $Z_{in} = k\eta H_0^{(2)}(kw/4)/4$ as given in Ref. [60]. Capacitive loads are obtained by means of a microstrip printed capacitances, as illustrated in Fig. 2 (a). Load-impedance density of printed capacitances can be approximated analytically using formulas for sheet impedance of a patch array [61] as it is done in [50], [53], [51], [54]. Although the analytical model represents a simple tool for designing metagratings, it takes into account the mutual coupling with adjacent loaded wires via a phenomenological scaling parameter which is found by means of 3D full-wave simulations of an entire supercell and, thus, is not unique. On the other hand, a recently developed simulation-based approach [56] allows one to construct metagrating unit cell by unit cell. Instead of performing computations on a whole supercell, it deals with a single unit cell and takes analytically into account the interaction between adjacent wires to retrieve load-impedance density. Additionally, simulation-based approaches are advantageous for being able to consider all practical aspects of meta-atoms, such as finite thickness of

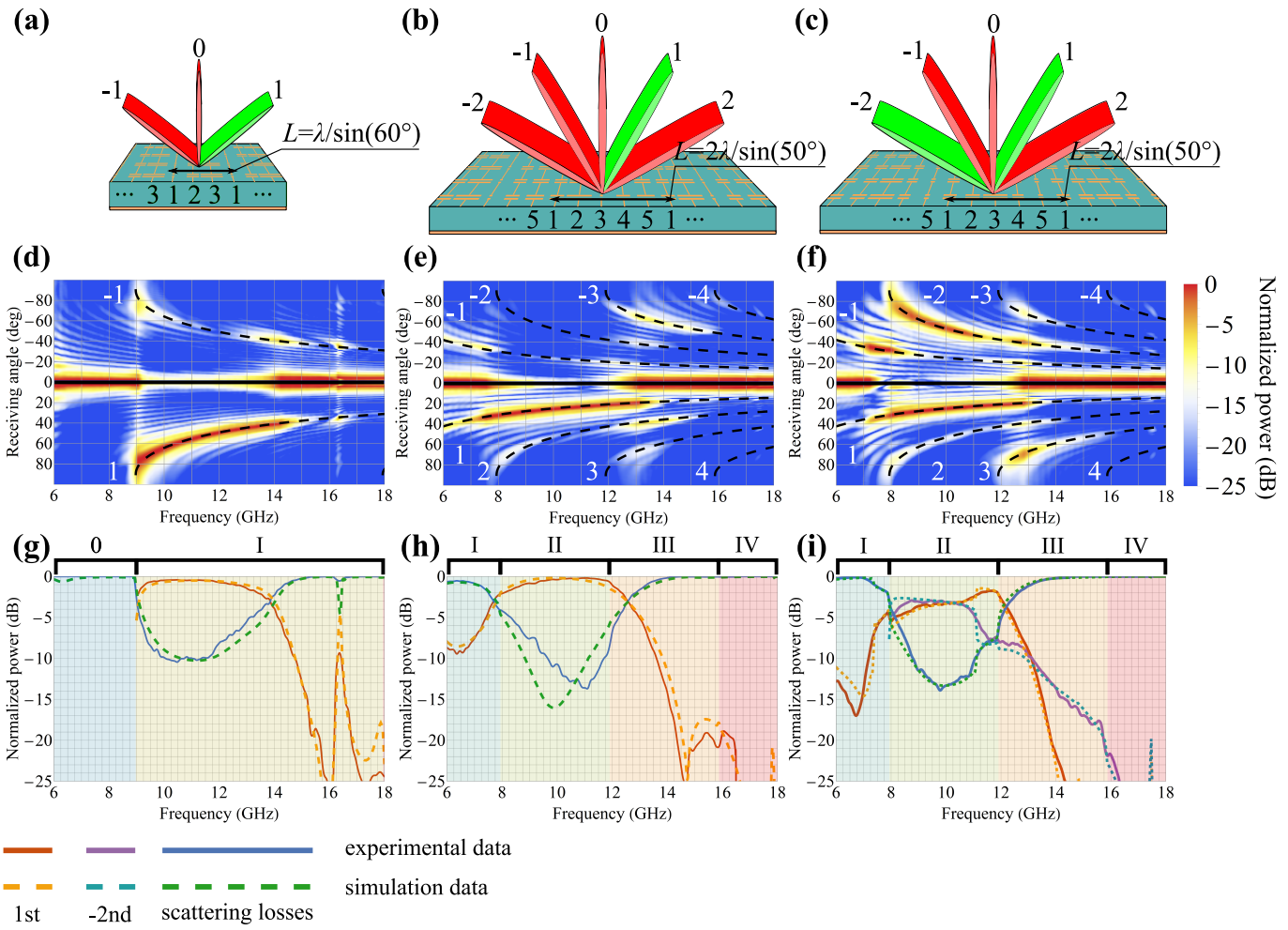

Fig. 3. (a)–(c) Schematics of prescribed diffraction patterns established by the three different designed metagratings with: (a) nonspecular reflection at an angle of 60° with $N = 3$ unit cells per period, (b) nonspecular reflection at an angle of 23° with $N = 5$ unit cells per period, and (c) equal excitation of the -2^{nd} and $+1^{\text{st}}$ orders out of five diffraction orders, respectively. The green and red beams correspond to excited and suppressed diffraction orders, respectively. (d)–(f) Measurement results of the scattered power in the [6 GHz – 18 GHz] frequency range. (g)–(i) Power management in the excited diffracting orders and scattering losses, the roman digits correspond to the highest propagating diffraction order in a given frequency range.

the metal cladding and conduction and dielectric losses.

We design three experimental samples of metagratings to operate at 10 GHz ($\lambda \approx 30$ mm) and we assume a normally incident plane-wave illumination ($\theta = 0$) for all three configurations. The functionalities of these three samples are schematically illustrated in Figs. 3 (a)–(c). The $h = 5$ mm thick F4BM220 dielectric substrate having permittivity $\varepsilon_s = 2.2(1 - j10^{-3})$ is selected as a good candidate for the proposed designs. The first sample deals with three diffraction orders maximizing the power scattered in the $+1^{\text{st}}$ order and suppressing scattering in the the -1^{st} and 0^{th} orders. Hence, it is composed of three unit cells per supercell, which has a length $L = \lambda/\sin(60°)$ at 10 GHz. This metagrating is able to achieve anomalous reflection at 60° degrees. The second and third samples each has five unit cells per supercell of length $L = 2\lambda/\sin(50°)$, which allows one to control five diffraction orders: -2^{nd}, -1^{st}, 0^{th}, $+1^{\text{st}}$ and $+2^{\text{nd}}$. The second sample maximizes the power scattered in the $+1^{\text{st}}$ propagating diffraction order and thus performs small angle anomalous reflection, corresponding approximately to 23° at 10 GHz. The third sample equally excites the -2^{nd} and $+1^{\text{st}}$ orders while suppressing the three others.

On the basis of these specifications, the required load-impedance density are calculated by means of Eqs. (1) – (3) and are presented in Table I. Only two capacitive unit cells of length $d = \lambda/[3\sin(60°)]$ and $d = 2\lambda/[5\sin(50°)]$ need to be simulated for the design of the three metagratings. A schematics of the unit cell is shown in Fig. 2 (a). In 3D full-wave simulations performed with COMSOL MULTI-PHYSICS, periodic boundary conditions are applied to the side faces of the unit cell and the model is excited with a periodic port. Parameters w and B are fixed to 0.25 mm and 3 mm, respectively. The arm's length A of the printed capacitance is used as a tuning parameter for the load-impedance density. The load-impedance densities are first extracted from the S_{11} parameter of the unit cell as detailed by the procedure in [56] and are plotted as function of A in Fig. 2 (b). Although being built for two different parameters d, the two curves in Fig. 2(b) almost coincide. It proofs that the analytical model used in Ref. [56] to take into account the interaction between

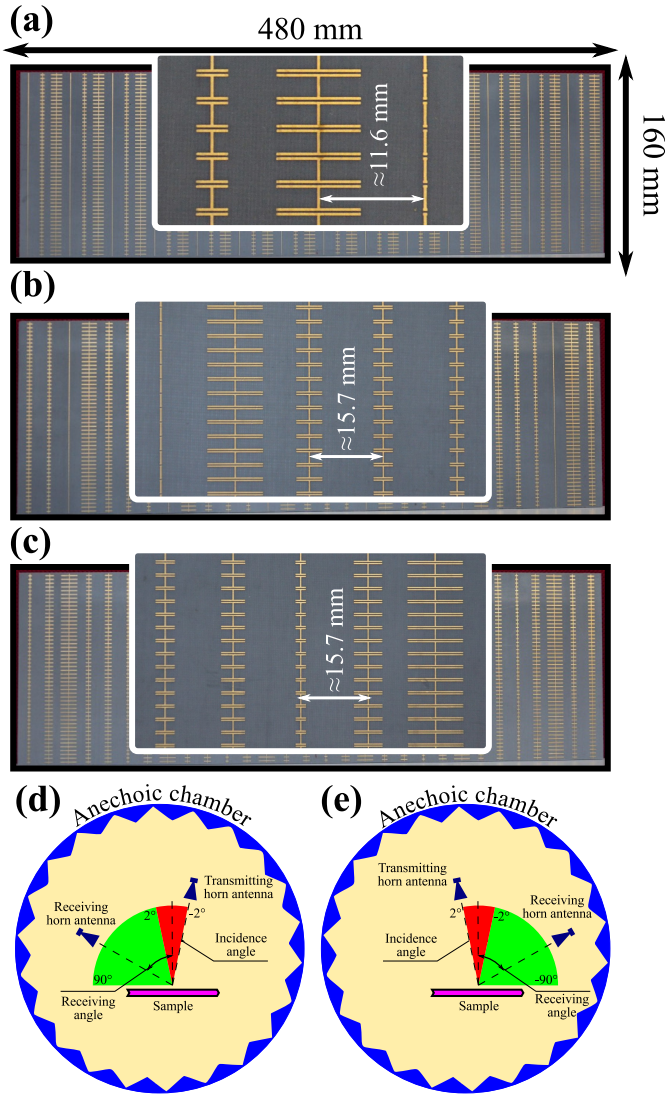

Fig. 4. (a)–(c) Photographies of the first, second and third samples (from top to bottom, respectively). (d), (e) Schematics of the experimental setup: to measure the scattering range of angles from $-90°$ to $90°$ the experiment is performed in the two steps illustrated by figures (d) and (e).

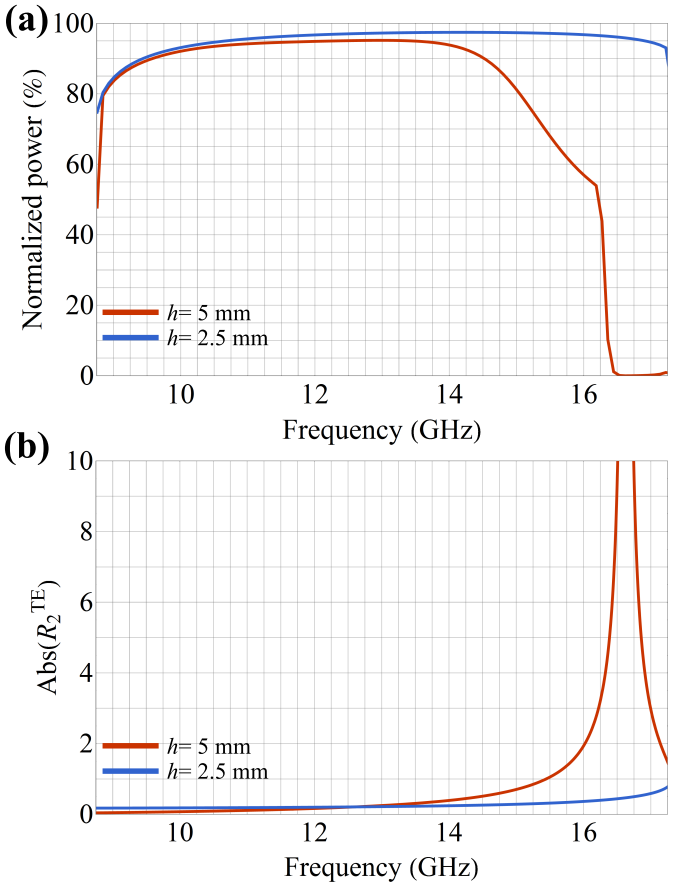

Fig. 5. (a) Computational results of the normalized power scattered by a reflective metagrating (having three reactive wires per period $L = \lambda/\sin(60°)$) in the $+1^{\text{st}}$ diffraction order vs. the frequency. Normally incident plane wave is assumed. Optimal reactive load-impedance densities are found at each frequency. (b) Absolute value of the Fresnel's reflection coefficient corresponding to the second (evanescent in the considered frequency range) diffraction order.

adjacent wires and the substrate, allows one to obtain the load-impedance density of a wire itself and not of a corresponding array. Eventually, the load-impedance densities are used to tailor the geometrical parameters of the microstrip printed capacitances listed in Table I. Photographies of the fabricated samples are displayed in Fig. 4 (a)–(c) and their physical size is approximately 480 mm (y-direction) by 160 mm (x-direction).

III. Experimental Results

In this section we demonstrate experimentally the control of diffraction patterns with the proposed and fabricated metagrating designs. The samples are tested in an anechoic chamber dedicated to radar-cross-section bistatic measurements, where transmitting and receiving horn antennas are mounted on a circular track of 5 m radius. A schematic representation of the experimental setup is shown in Figs. 4 (d) and (e). In the current experiments, the transmitter is fixed and the receiver moves with $1°$ step and the minimum angle between the transmitter and receiver for the scanning is $4°$. In order to be able to measure the specular reflection, the transmitter is fixed at $\mp 2°$. Thus, the experiments are conducted in two steps: when the transmitter is fixed at $\mp 2°$, the receiver moves form $\pm 2°$ to $\pm 90°$, as it is clearly illustrated in Figs. 4 (d) and (e).

Figures 3(d)–(f) visualize angle measurements of the scattered power in the frequency range spanning from 6 to 18 GHz. It is clearly observed that the positions of the main lobes (corresponding to diffraction orders) are in perfect agreement with the results given by the grating formula $\theta_m = \sin^{-1}(mc/(\nu L) + \sin[\theta_i])$ (represented by black dashed curves). Here, c is the speed of light in vacuum and ν is the frequency. However, the spectrum of waves scattered from a finite-size sample in the far-field is much more complex than just a few plane waves representing propagating diffraction orders. Thus, in order to estimate the performance of the samples we execute next steps following Ref. [52]. In the first place, we localize each diffraction order between the angles $\theta_m^{(1)}$ and $\theta_m^{(2)}$ which correspond to 3 dB of the power attenuation with respect to the maximum power of the lobe. The maximum is found near the angle $\theta_m = \sin^{-1}(mc/(\nu L) + \sin[\theta_i])$. Finally,

the normalized power $f_m(\nu)$ scattered in a given diffraction order m at the frequency ν is estimated by means of the following integral formula

$$f_m(\nu) = \frac{\int_{\theta_m^{(1)}}^{\theta_m^{(2)}} P(\nu,\theta)d\theta}{\sum_m \int_{\theta_m^{(1)}}^{\theta_m^{(2)}} P(\nu,\theta)d\theta}, \quad (4)$$

where $P(\nu,\theta)$ is the absolute power scattered in the receiving angle θ at the frequency ν. The summation in the denominator is performed over all propagating diffraction orders at the frequency ν. Figures 3(g)–(i) show the performance of the experimental samples (solid curves obtained by means of Eq. (4)) as function of the frequency, scattering losses represent the power scattered in undesired diffraction orders. The dashed curves demonstrate the results obtained from 3D full-wave simulations (a supercell with imposed periodic boundary conditions and excited by a periodic port). By comparing the solid and dashed curves, one can observe a good agreement between the experimental and simulation results.

Although the samples were designed to operate at a single frequency (10 GHz), it is seen that the scattering losses remain low in a wide range of frequencies. One of the most important factors affecting an operating frequency range is the frequency response of unit cells. Resonant elements, in a general manner, significantly decrease an operating frequency range (see, e.g., Refs. [54], [56]). As demonstrated by Fig. 2(b), unit cells used to construct experimental samples do not exhibit resonances at 10 GHz. Since the designed metagratings possess a number of degrees of freedom equal to the number of propagating diffraction orders, it is expected that the scattering losses increase when approaching frequencies where the number of propagating diffraction orders changes (corresponding to different areas in Figs. 3(g)–(i) labeled with roman digits). While it is the case for the second and third samples, the performance of the first one decreases far before the appearance of the second propagating diffraction orders, see Figs. 3(g)–(i). It unveils yet another crucial factor influencing an operating frequency range: excitation of waveguide modes discussed in the very beginning of Section II. Although we avoid waveguide modes around the design frequency of 10 GHz, they may appear at lower or higher frequencies and this is exactly what happens with the first sample, as we further present in Fig. 5. A waveguide mode is excited at the frequency when the Fresnel's reflection coefficient R_2^{TE} diverges and leads to drastic decrease of the performance of the metagrating, as it can be clearly observed in Fig. 5 when comparing two different thicknesses of the dielectric substrate. In the experimental and simulation data the waveguide mode manifests itself in the resonance observed around 16.4 GHz, see Figs. 3(d) and (g). Figure 5(a) presents the computational results of maximizing the power of a normally incident plane wave coupled to the $+1^{\mathrm{st}}$ propagating diffraction order in the three unit cells per period metagrating, assuming purely reactive load-impedance densities. As demonstrated, the excitation of the waveguide mode can be suppressed by choosing a thinner substrate (for e.g. 2.5 mm instead of 5 mm) which enables restoring the performance over the entire range of frequencies where there are three propagating diffraction orders (see blue curves in Fig. 5).

IV. CONCLUSION

To conclude, we have described in details the design procedure of reflective metagratings and tested three experimental samples able of establishing prescribed diffraction pattern in a wide frequency range. The experimental results have demonstrated a good agreement with 3D full-wave simulations. Thus, we have experimentally verified the concept of metagratings for controlling multiple beams with as few as one degree of freedom (represented by a reactive load) per a propagating diffraction order. We have identified the main factors affecting the operating frequency range of metagratings which should facilitate the development of wide-band beamforming devices in the future.

ACKNOWLEDGEMENTS

The authors acknowledge the help of Anil Cheraly (ONERA) in conducting the experiments.

REFERENCES

[1] M. Born, E. Wolf, A. B. Bhatia, P. C. Clemmow, D. Gabor, A. R. Stokes, A. M. Taylor, P. A. Wayman, and W. L. Wilcock, *Principles of Optics: Electromagnetic Theory of Propagation, Interference and Diffraction of Light*, 7th ed. Cambridge University Press, 1999, ch. Elements of the theory of diffraction, pp. 412 – 516.

[2] F. P. Schäfer, *Dye Lasers*, 3rd ed. Springer-Verlag Berlin Heidelberg, 1990.

[3] F. Duarte and L. W. Hillman, *Dye Laser Principles*. San Diego: Academic Press, 1990, ch. Narrow-linewidth pulsed dye laser oscillators, pp. 133 – 183.

[4] E. V. Jull, J. W. Heath, and G. R. Ebbeson, "Gratings that diffract all incident energy," *J. Opt. Soc. Am.*, vol. 67, no. 4, pp. 557–559, Apr 1977.

[5] A. Hessel, J. Schmoys, and D. Y. Tseng, "Bragg-angle blazing of diffraction gratings," *J. Opt. Soc. Am.*, vol. 65, no. 4, pp. 380–384, Apr 1975.

[6] E. V. Jull, N. C. Beaulieu, and D. C. W. Hui, "Perfectly blazed triangular groove reflection gratings," *J. Opt. Soc. Am. A*, vol. 1, no. 2, pp. 180–182, Feb 1984.

[7] J. Shmoys and A. Hessel, "Analysis and design of frequency scanned transmission gratings," *Radio Science*, vol. 18, no. 04, pp. 513–518, July 1983.

[8] F. S. Johansson, "A new planar grating-reflector antenna," *IEEE Transactions on Antennas and Propagation*, vol. 38, no. 9, pp. 1491–1495, Sep. 1990.

[9] F. S. Johansson, L. R. Lagerholm, and P.-S. Kildal, "Frequency-scanned reflection gratings with integrated polarizer," *IEEE Transactions on Antennas and Propagation*, vol. 40, no. 3, pp. 331–334, March 1992.

[10] R. Lagerholm, "Study of metallic strip gratings for frequency scanning," *Microwave and Optical Technology Letters*, vol. 5, no. 14, pp. 713–715, 1992.

[11] T. Mathew, D. S. Stephen, K. A. Jose, C. K. Aanandan, P. Mohanan, and K. G. Nair, "The performance of a novel simulated corrugated surface for the reduction of radar cross section," *Microwave and Optical Technology Letters*, vol. 6, no. 10, pp. 615–617, 1993.

[12] D. S. Stephen, T. Mathew, P. Mohanan, and K. G. Nair, "A modified strip grating with dual periodicity for rcs reduction," *Microwave and Optical Technology Letters*, vol. 7, no. 7, pp. 315–317, 1994.

[13] H. Lotem, "Littrow-mounted diffraction grating cavity," *Appl. Opt.*, vol. 33, no. 6, pp. 930–934, Feb 1994.

[14] T. Itoh and R. Mittra, "An analytical study of the echelette grating with application to open resonators," *IEEE Transactions on Microwave Theory and Techniques*, vol. 17, no. 6, pp. 319–327, June 1969.

[15] C. L. Holloway, E. F. Kuester, J. A. Gordon, J. O'Hara, J. Booth, and D. R. Smith, "An overview of the theory and applications of metasurfaces: The two-dimensional equivalents of metamaterials," *IEEE Antennas and Propagation Magazine*, vol. 54, no. 2, pp. 10–35, April 2012.

[16] N. Yu and F. Capasso, "Flat optics with designer metasurfaces," *Nature materials*, vol. 13, no. 2, p. 139, 2014.

[17] N. Yu, P. Genevet, M. A. Kats, F. Aieta, J.-P. Tetienne, F. Capasso, and Z. Gaburro, "Light propagation with phase discontinuities: generalized laws of reflection and refraction," *Science*, vol. 334, no. 6054, pp. 333–337, 2011.

[18] X. Ni, N. K. Emani, A. V. Kildishev, A. Boltasseva, and V. M. Shalaev, "Broadband light bending with plasmonic nanoantennas," *Science*, vol. 335, no. 6067, pp. 427–427, 2012.

[19] F. Aieta, P. Genevet, N. Yu, M. A. Kats, Z. Gaburro, and F. Capasso, "Out-of-plane reflection and refraction of light by anisotropic optical antenna metasurfaces with phase discontinuities," *Nano Letters*, vol. 12, no. 3, pp. 1702–1706, 2012.

[20] S. Sun, K.-Y. Yang, C.-M. Wang, T.-K. Juan, W. T. Chen, C. Y. Liao, Q. He, S. Xiao, W.-T. Kung, G.-Y. Guo, L. Zhou, and D. P. Tsai, "High-efficiency broadband anomalous reflection by gradient meta-surfaces," *Nano Letters*, vol. 12, no. 12, pp. 6223–6229, 2012.

[21] A. Díaz-Rubio, V. S. Asadchy, A. Elsakka, and S. A. Tretyakov, "From the generalized reflection law to the realization of perfect anomalous reflectors," *Science Advances*, vol. 3, no. 8, 2017.

[22] V. S. Asadchy, A. Díaz-Rubio, S. N. Tcvetkova, D.-H. Kwon, A. Elsakka, M. Albooyeh, and S. A. Tretyakov, "Flat engineered multichannel reflectors," *Phys. Rev. X*, vol. 7, p. 031046, Sep 2017.

[23] C. Pfeiffer and A. Grbic, "Metamaterial huygens' surfaces: Tailoring wave fronts with reflectionless sheets," *Phys. Rev. Lett.*, vol. 110, p. 197401, May 2013.

[24] F. Monticone, N. M. Estakhri, and A. Alù, "Full control of nanoscale optical transmission with a composite metascreen," *Phys. Rev. Lett.*, vol. 110, p. 203903, May 2013.

[25] M. Kim, A. M. H. Wong, and G. V. Eleftheriades, "Optical huygens' metasurfaces with independent control of the magnitude and phase of the local reflection coefficients," *Phys. Rev. X*, vol. 4, p. 041042, Dec 2014.

[26] Y. Yuan, K. Zhang, X. Ding, B. Ratni, S. N. Burokur, and Q. Wu, "Complementary transmissive ultra-thin meta-deflectors for broadband polarization-independent refractions in the microwave region," *Photon. Res.*, vol. 7, no. 1, pp. 80–88, Jan 2019.

[27] X. Chen, L. Huang, H. Mühlenbernd, G. Li, B. Bai, Q. Tan, G. Jin, C.-W. Qiu, S. Zhang, and T. Zentgraf, "Dual-polarity plasmonic metalens for visible light," *Nature communications*, vol. 3, p. 1198, 2012.

[28] F. Aieta, P. Genevet, M. A. Kats, N. Yu, R. Blanchard, Z. Gaburro, and F. Capasso, "Aberration-free ultrathin flat lenses and axicons at telecom wavelengths based on plasmonic metasurfaces," *Nano Letters*, vol. 12, no. 9, pp. 4932–4936, 2012.

[29] X. Ni, S. Ishii, A. V. Kildishev, and V. M. Shalaev, "Ultra-thin, planar, babinet-inverted plasmonic metalenses," *Light: Science & Applications*, vol. 2, no. 4, p. e72, 2013.

[30] X. Ding, F. Monticone, K. Zhang, L. Zhang, D. Gao, S. N. Burokur, A. de Lustrac, Q. Wu, C.-W. Qiu, and A. Alù, "Ultrathin pancharatnam-berry metasurface with maximal cross-polarization efficiency," *Advanced Materials*, vol. 27, no. 7, pp. 1195–1200, 2015.

[31] A. Alù and N. Engheta, "Achieving transparency with plasmonic and metamaterial coatings," *Phys. Rev. E*, vol. 72, p. 016623, Jul 2005.

[32] P.-Y. Chen, C. Argyropoulos, and A. Alù, "Broadening the cloaking bandwidth with non-foster metasurfaces," *Phys. Rev. Lett.*, vol. 111, p. 233001, Dec 2013.

[33] T. V. Teperik, S. N. Burokur, A. de Lustrac, G. Sabanowski, and G.-P. Piau, "Experimental validation of an ultra-thin metasurface cloak for hiding a metallic obstacle from an antenna radiation at low frequencies," *Applied Physics Letters*, vol. 111, no. 5, p. 054105, 2017.

[34] S. Sun, Q. He, S. Xiao, Q. Xu, X. Li, and L. Zhou, "Gradient-index meta-surfaces as a bridge linking propagating waves and surface waves," *Nature materials*, vol. 11, no. 5, p. 426, 2012.

[35] S. N. Tcvetkova, D.-H. Kwon, A. Díaz-Rubio, and S. A. Tretyakov, "Near-perfect conversion of a propagating plane wave into a surface wave using metasurfaces," *Phys. Rev. B*, vol. 97, p. 115447, Mar 2018.

[36] L. Huang, X. Chen, H. Mühlenbernd, G. Li, B. Bai, Q. Tan, G. Jin, T. Zentgraf, and S. Zhang, "Dispersionless phase discontinuities for controlling light propagation," *Nano Letters*, vol. 12, no. 11, pp. 5750–5755, 2012.

[37] M. Q. Mehmood, S. Mei, S. Hussain, K. Huang, S. Y. Siew, L. Zhang, T. Zhang, X. Ling, H. Liu, J. Teng, A. Danner, S. Zhang, and C.-W. Qiu, "Visible-frequency metasurface for structuring and spatially multiplexing optical vortices," *Advanced Materials*, vol. 28, no. 13, pp. 2533–2539, 2016.

[38] G. Li, L. Wu, K. F. Li, S. Chen, C. Schlickriede, Z. Xu, S. Huang, W. Li, Y. Liu, E. Y. B. Pun, T. Zentgraf, K. W. Cheah, Y. Luo, and S. Zhang, "Nonlinear metasurface for simultaneous control of spin and orbital angular momentum in second harmonic generation," *Nano Letters*, vol. 17, no. 12, pp. 7974–7979, 2017.

[39] K. Zhang, Y. Yuan, D. Zhang, X. Ding, B. Ratni, S. N. Burokur, M. Lu, K. Tang, and Q. Wu, "Phase-engineered metalenses to generate converging and non-diffractive vortex beam carrying orbital angular momentum in microwave region," *Opt. Express*, vol. 26, no. 2, pp. 1351–1360, Jan 2018.

[40] Y. Yifat, M. Eitan, Z. Iluz, Y. Hanein, A. Boag, and J. Scheuer, "Highly efficient and broadband wide-angle holography using patch-dipole nanoantenna reflectarrays," *Nano Letters*, vol. 14, no. 5, pp. 2485–2490, 2014.

[41] D. Wen, F. Yue, G. Li, G. Zheng, K. Chan, S. Chen, M. Chen, K. F. Li, P. W. H. Wong, K. W. Cheah, E. Y. B. Pun, S. Zhang, and X. Chen, "Helicity multiplexed broadband metasurface holograms," *Nature communications*, vol. 6, p. 8241, 2015.

[42] X. Li, L. Chen, Y. Li, X. Zhang, M. Pu, Z. Zhao, X. Ma, Y. Wang, M. Hong, and X. Luo, "Multicolor 3d meta-holography by broadband plasmonic modulation," *Science Advances*, vol. 2, no. 11, 2016.

[43] X. Ni, A. V. Kildishev, and V. M. Shalaev, "Metasurface holograms for visible light," *Nature communications*, vol. 4, p. 2807, 2013.

[44] W. Wan, J. Gao, and X. Yang, "Metasurface holograms for holographic imaging," *Advanced Optical Materials*, vol. 5, no. 21, p. 1700541, 2017.

[45] Z. Wang, X. Ding, K. Zhang, B. Ratni, S. N. Burokur, X. Gu, and Q. Wu, "Huygens metasurface holograms with the modulation of focal energy distribution," *Advanced Optical Materials*, vol. 6, no. 12, p. 1800121, 2018.

[46] V. S. Asadchy, M. Albooyeh, S. N. Tcvetkova, A. Díaz-Rubio, Y. Ra'di, and S. A. Tretyakov, "Perfect control of reflection and refraction using spatially dispersive metasurfaces," *Phys. Rev. B*, vol. 94, p. 075142, Aug 2016. [Online]. Available: https://link.aps.org/doi/10.1103/PhysRevB.94.075142

[47] N. M. Estakhri and A. Alù, "Wave-front transformation with gradient metasurfaces," *Physical Review X*, vol. 6, no. 4, pp. 1–17, 2016.

[48] A. Epstein and G. V. Eleftheriades, "Huygens' metasurfaces via the equivalence principle: design and applications," *J. Opt. Soc. Am. B*, vol. 33, no. 2, pp. A31–A50, Feb 2016.

[49] Y. Ra'di, D. L. Sounas, and A. Alù, "Metagratings: Beyond the limits of graded metasurfaces for wave front control," *Phys. Rev. Lett.*, vol. 119, p. 067404, Aug 2017.

[50] A. Epstein and O. Rabinovich, "Unveiling the properties of metagratings via a detailed analytical model for synthesis and analysis," *Phys. Rev. Applied*, vol. 8, p. 054037, Nov 2017.

[51] O. Rabinovich and A. Epstein, "Analytical design of printed circuit board (pcb) metagratings for perfect anomalous reflection," *IEEE Transactions on Antennas and Propagation*, vol. 66, no. 8, pp. 4086–4095, Aug 2018.

[52] O. Rabinovich, I. Kaplon, J. Reis, and A. Epstein, "Experimental demonstration and in-depth investigation of analytically designed anomalous reflection metagratings," *Phys. Rev. B*, vol. 99, p. 125101, Mar 2019.

[53] V. Popov, F. Boust, and S. N. Burokur, "Controlling diffraction patterns with metagratings," *Phys. Rev. Applied*, vol. 10, p. 011002, Jul 2018. [Online]. Available: https://link.aps.org/doi/10.1103/PhysRevApplied.10.011002

[54] ——, "Constructing the near field and far field with reactive metagratings: Study on the degrees of freedom," *Phys. Rev. Applied*, vol. 11, p. 024074, Feb 2019. [Online]. Available: https://link.aps.org/doi/10.1103/PhysRevApplied.11.024074

[55] L. B. Felsen and N. Marcuvitz, *Radiation and scattering of waves*. John Wiley & Sons, 1994, vol. 31.

[56] V. Popov, M. Yakovleva, F. Boust, J.-L. Pelouard, F. Pardo, and S. N. Burokur, "Designing metagratings via local periodic approximation: From microwaves to infrared," *Phys. Rev. Applied*, vol. 11, p. 044054, Apr 2019.

[57] A. Epstein and O. Rabinovich, "Perfect anomalous refraction with metagratings," *IET Conference Proceedings*, p. 479 (5 pp.), January 2018.

[58] A. Díaz-Rubio, V. S. Asadchy, A. Elsakka, and S. A. Tretyakov, "From the generalized reflection law to the realization of perfect anomalous reflectors," *Science Advances*, vol. 3, no. 8, 2017.

[59] A. Epstein and G. V. Eleftheriades, "Synthesis of passive lossless metasurfaces using auxiliary fields for reflectionless beam splitting and perfect reflection," *Phys. Rev. Lett.*, vol. 117, p. 256103, Dec 2016. [Online]. Available: https://link.aps.org/doi/10.1103/PhysRevLett.117.256103

[60] S. Tretyakov, *Analytical modeling in applied electromagnetics*. Artech House, 2003.

[61] O. Luukkonen, C. Simovski, G. Granet, G. Goussetis, D. Lioubtchenko, A. V. Raisanen, and S. A. Tretyakov, "Simple and accurate analytical model of planar grids and high-impedance surfaces comprising metal strips or patches," *IEEE Transactions on Antennas and Propagation*, vol. 56, no. 6, pp. 1624–1632, June 2008.